



*Research article*

## **Mechanical properties of sandwich composite made of syntactic foam core and GFRP skins**

**Zulzamri Salleh<sup>1,2</sup>, Md Mainul Islam<sup>1,\*</sup>, Jayantha Ananda Epaarachchi<sup>1</sup>, and Haibin Su<sup>3</sup>**

<sup>1</sup> Centre for Future Materials (CFM) and School of Mechanical and Electrical Engineering, Faculty of Health, Engineering and Sciences, University of Southern Queensland, Toowoomba, Queensland 4350, Australia

<sup>2</sup> University Kuala Lumpur, Malaysian Institute of Marine Engineering Technology, 32200, Lumut, Perak, Malaysia

<sup>3</sup> Division of Materials Science, Nanyang Technological University, 50 Nanyang Avenue, Singapore 639798

\* **Correspondence:** Email: [Mainul.Islam@usq.edu.au](mailto:Mainul.Islam@usq.edu.au).

**Abstract:** Sandwich composites or sandwich panels have been widely used as potential materials or building structures and are regarded as a lightweight material for marine applications. In particular, the mechanical properties, such as the compressive, tensile and flexural behaviour, of sandwich composites formed from glass fibre sheets used as the skin and glass microballoon/vinyl ester as the syntactic foam core were investigated in this report. This syntactic foam core is sandwiched between unidirectional glass fibre reinforced plastic (GFRP) using vinyl ester resins to build high performance sandwich panels. The results show that the compressive and tensile strengths decrease when the glass microballoon content is increased in syntactic foam core of sandwich panels. Moreover, compressive modulus is also found to be decreased, and there is no trend for tensile modulus. Meanwhile, the flexural stiffness and effective flexural stiffness for edgewise position have a higher bending as 50% and 60%, respectively. Furthermore, the results indicated that the glass microballoon mixed in a vinyl ester should be controlled to obtain a good combination of the tensile, compressive and flexural strength properties.

---

**Keywords:** syntactic foam; composite sandwich panel; glass microballoon; resin; tensile; flexural

---

## 1. Introduction

Nowadays composite sandwich panels made of foam are preferred, especially in construction engineering applications as structural insulated panel layer, a thin layer of carbon fibre reinforced plastic or a thick foam protector [1,2]. Approximately 50 years ago, the conceptual sandwich structure was studied by several researchers, e.g., [3], Allen [4], Gay and Hoe [5]. Additionally, it is often used in marine, aerospace and automotive industries, where low weight is an important major factor in the design that can be developed [6,7]. Previous report also indicated that performance of marine sandwich composite panels with particularly selected mechanical properties can be enhanced by using glass microballoon syntactic foams as core materials [8]. Core materials with higher volume fraction of glass microballoon in matrix resin contribute to weight saving properties. However, it may lead to lower strength properties unless a careful consideration is imposed when designing with GFRP skins. The design concept behind composite sandwich panel construction is that the skin carries the in-plane compressive load while the primary function of the light weight syntactic foam core is to maintain the GFRP skins at a desired distance. In this study, the skin of the sandwich panel consists of a mixture of GFRP with a vinyl ester resin acting as a binder. Furthermore, sandwich panels can be developed using GFRP as the skin and polyol-isocyanate foam as the core, which have been previously used as entry doors and partitions [9].

In another study, Mostafa et al. [10] developed sandwich panels using PVC closed cell foams as the core with a GFRP face sheet with different layers and epoxy resin as the binder. Generally, core foams use a polymer resin, such as epoxy resin, cyanate ester, polypropylene, polysialate and vinyl ester as well as other polymer resins [11] as the matrix materials. Among all of the polymer matrix materials mentioned above, epoxy matrix syntactic foams are widely studied due to the extensive use of epoxy resins in aerospace applications [12–17]. When demand is high for this resin, especially due to the price of composites in the market, an alternative resin needs to be obtained that has similar behaviour but does not compromise in mechanical properties. Vinyl ester is a better choice in terms of competitive price and widely used in marine applications [18–21]. Therefore, investigating the properties of vinyl ester matrix binder core foams and developing structure–property correlations for these materials are important challenges. Sandwich panels with higher strength and stiffness for thin skin is more preferable in early 20 centuries particularly used in aerospace, automotive and marine applications [22]. Various findings have been found when sandwich panels made from metal and GFRP skin were studied by many researchers [23]. The sandwich panels using carbon-FRP skin also fabricated by Shawkat et al. with injection moulding method and found many bubbles between core and skin area [24]. Islam and Kim found that the mechanical properties are also affected by bonding condition between starch core and paper skin of sandwich panels by a parametric study on constituent materials [25]. Ziad et al. also found that the de-bonding failure mode was occurred in glue-laminated GFRP sandwich beams which are contributed to the higher flexural bending stiffness [26].

Furthermore, the contribution to the knowledge of the syntactic foam as the core material can also be expanded by using different foam cores such as polyurethane foam [10,22,27,28], polypropylene and polystyrene foam [10,29] and aluminium foam [30,31,32]. A previous report stated that the strength of a core foam is limited to the composite behaviour of its sandwich structure; thus, the core density and thickness were varied to include the range of manufacturing specification values [33]. The reports highlighted that the characterisation of the mechanical properties of the core foam was affected by both properties [34,35]. In previous studies, several researchers were interested in the properties of the foams, particularly on the compressive strength and the absorbed energy, i.e., a stress plateau, which is a typical feature for most types of syntactic foams [36]. In this test, the plateau can be subdivided into a linear elastic region in the early stages during the densification region prior to failure. Viot et al. [37] observed that the compressive testing result of polypropylene foams at several densities and strain rates indicated that the stress plateau increased with higher stress values.

Other researchers also found that the same phenomenon occurs in their findings [16,38]. In the tensile testing on a composite sandwich panel, it is important to measure the strength of both skins. However, the syntactic core foam also affects the tensile value when the material is more brittle [27]. Similar to other testing, the tensile measurement depends significantly on the material density, strain-rate loading, temperature and humidity [9]. Zhang et al. [27] using different strain rates and temperatures indicated that the low density foam core completely changes the behaviour by its constituent materials. Furthermore, the density of the core foams was one of the primary items that needed to be investigated in flexural testing. Sharaf et al. [24] determined that the flexural performance could be enhanced by increasing the density of the polyurethane core foams in the sandwich panels. Additionally, Nambiar and Ramamurthy [39] investigated the flexural performance using GFRP-sandwich panels with a soft polyurethane core to estimate the deflection and compared it to conventional reinforced concrete. In this study, four stages were created to investigate the syntactic sandwich panels, (a) the preparation of skin sandwich panels made of glass fibre reinforced plastic (GFRP), (b) the fabrication of sandwich panels using syntactic foam as core material and GFRP as skin material, (c) investigation of their mechanical behaviour in relation to the constituents' properties and fabrication conditions, and (d) characterisation of the fracture mechanism of the syntactic foams and a microstructure analysis using a scanning electron microscope (SEM).

## **2. Materials and Method**

### *2.1. Constituent Materials*

The vinyl ester resin, which has a scientific name of diglycidyl ether of bisphenol A-based resin, and a methyl ethyl ketone peroxide (MEKP) catalyst, which was used as the matrix material, were procured from Nuplex Industries (Australia) Pty Ltd, to use in this study. The glass microballoons used in this study are non-porous in nature and manufactured and supplied by Potters Industries Inc. under the trade name of Q-CEL Spherical (R) Hollow Microspheres. In this study, the physical shape of the glass microballoon consists of spherical glass powder typed with a chemically stable fused-borosilicate glass and a non-porous microsphere.

The mean inner diameter is calculated by taking the difference in the average true particle density of the solid and hollow particles consisting of the same material. The particle size density was measured to be 0.19 g/cc whereas the bulk density was 0.11 g/cc. The particle size was measured to be 72  $\mu\text{m}$  on average, and the size ranged from 5–150  $\mu\text{m}$ . The syntactic foam used as the core material consisted of the glass microballoon, and the matrix resin used in this study was vinyl ester. The compositions of the glass microballoons were varied for the core of the sandwich panel: 2 wt%, 4 wt%, 6 wt%, 8 w% and 10 wt%. Three replicates from each of these composition types were tested for each of compressive, tensile and flexural testing.

## 2.2. Fabrication of GFRP Sheet

The fabrication of the syntactic foams sandwich panels was prepared in two stages, i.e., the pre-mould process. The first preparation is to prepare the skin syntactic foam sandwich panels. The hand layup technique was used in this study to apply the vinyl ester resin to the unidirectional GFRP. The size of the GFRP was cut into 370 mm  $\times$  400 mm and stacked at a 3-layer thickness. It was then placed onto the rectangular shape glass as the bottom base, and the vinyl ester was poured on it using a small squeegee to facilitate uniform resin distribution and the removal of air pockets [10]. Then, the top of this area was covered by a rectangular-shaped glass to ensure a uniform flatness. Furthermore, a small weight was pushed onto the glass until the vinyl ester spread to the edge of the rectangular glass. The GFRP was cured at room temperature for 24 hours at a humidity of 85%RH. The re-moulding process was performed after it was cured, and it was then placed into an oven for final curing at a temperature of 80  $^{\circ}\text{C}$ .

## 2.3. Compressive Sandwich Panel Specimens

The second preparation involved fabricating the syntactic foam as a core using sandwich syntactic foam materials. The types of specimens depended on the mechanical properties that needed to be investigated for the sandwich panels. Shen et al. performed three types of testing on sandwich panel foams, which involved compression, tensile and flexural testing [9]. In this study, the ASTM standard applied in the compression test is ASTM C-365. Cylindrical-shaped PVC tubes with dimensions of diameter  $\phi = 30.0$  mm and length  $L = 60.0$  mm were used for the compression moulds in this study. First, the moulds had to be cleaned using acetone, and the surface was coated with mould wax to ensure that the syntactic foams could be easily removed. The GFRP skin was placed at the bottom of the PVC mould with masking tape as a seal to avoid slurry leakage. This synthesis method consists of mixing different measured quantities of glass microballoons in the vinyl ester resin and stir mixing them until a slurry of uniform viscosity is obtained. The mixing time is approximately 4 to 5 min.

Then, the required number of glass microballoons, based on the weight percentage, was weighed separately and added slowly to the resin mixture. The mixture was then transferred to a PVC mould. The specimens along with the mould were allowed to cure for 24 hours at room temperature and then removed from the mould. The fabrication of the compressive specimens is

depicted in Figure 1. To ensure complete curing, the sample was then post-cured at 80 °C for 4 hours in a hot air oven.

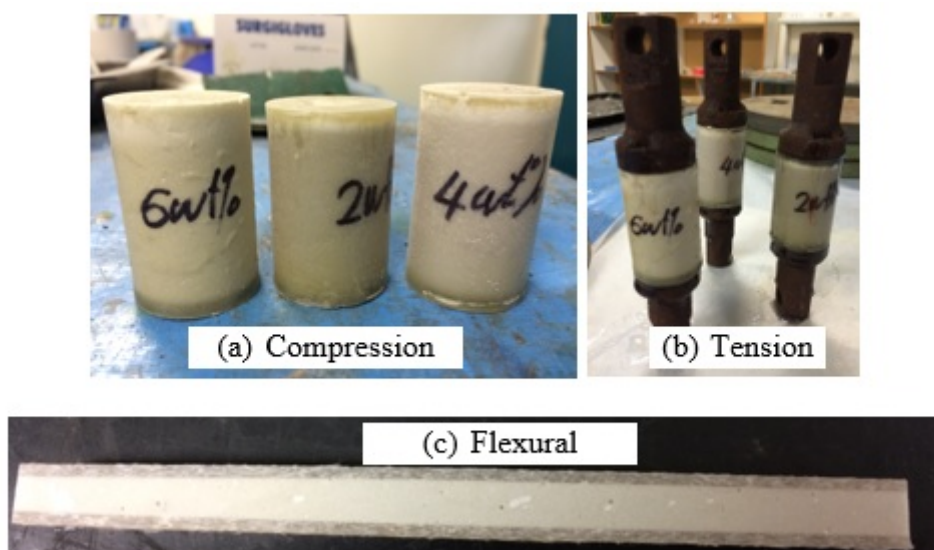


**Figure 1.** Representative specimens of syntactic foam sandwich panels.

The compression test was performed using MTS test systems with a constant test speed of 2 mm/min. Figure 2 depicts the photograph of one of the specimens tested during the compression test in the MTS machine. From the output result, two parameters have been selected for data analysis, such as the load and crosshead displacement, to develop the stress-strain curves. Then, it is necessary to re-calculate the actual values of stress and strain using the area formula for a cylindrical shape for each sample.

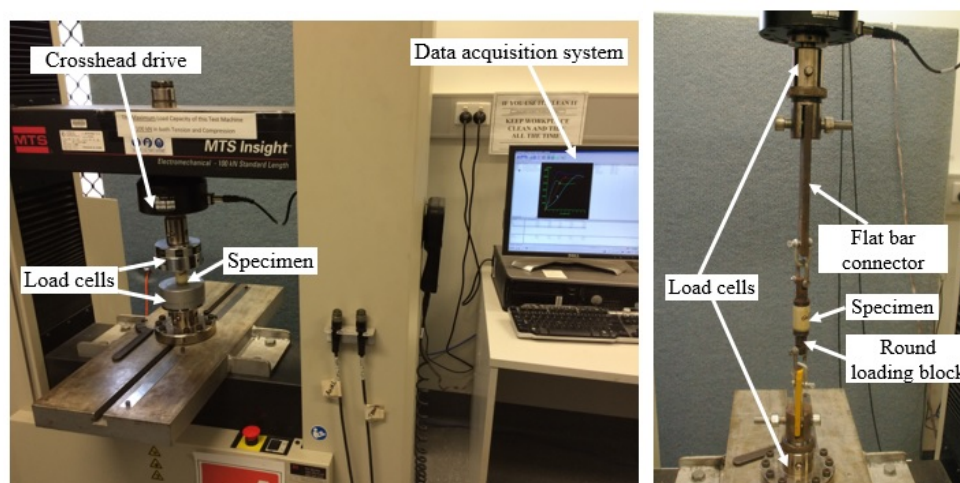


**Figure 2.** Representative overview of the mechanical testing setup using the MTS Insight machine.

#### 2.4. Tensile Sandwich Panel Specimens

The tensile specimens for this study follow the dimension size from the compression sample size and are based on ASTM C297. Similar to the compressive specimens, the GFRP skin sticks together on the top and the bottom while the slurry is poured and mixed with the vinyl ester resin. The evaporation from the styrene gas produced from the MEKP hardener makes it difficult for the skin to stick to the top of the syntactic foam cores. Therefore, a rectangular glass plate has been placed on top of all of the specimens while being cured at room temperature, 25 °C. After the remoulding process, all of the specimens were pasted to the tensile loading bloc using an epoxy adhesive type techniglu R5 mixed with hardener techniglu H5 at a concentration ratio of (1:1). The detailed representative specimens for the drying process at room temperature, T: 25 °C/RH 75%, are illustrated in Figure 1.

#### 2.5. Flexural Shear Sandwich Panel Specimens

Additionally, the specimens for the flexural sandwich syntactic foam core are prepared from the same skin as the GFRP compressive specimens. The sandwich panels for the GFRP skin syntactic foam core were prepared based on ASTM C 393/393M-11. This method is required for a 3-point loading (TPB) with a mid-span and a total span length supported at 150 mm. Similar to the preparation for compressive core syntactic foam, the glass microballoon was measured with different weight percentages before it was poured and cast into the GFRP skin. The GFRP skin for both sides were stuck to each other using masking tape.

### 3. Results

#### 3.1. Compressive Properties

The specimens can be identified as SCSW-1, SCSW-2, SCSW-3, SCSW-4 and SCSW-5 for syntactic foam cores with glass microballoon contents of 2 wt%, 4 wt%, 6 wt%, 8 wt% and 10 wt%, respectively. The properties of the syntactic foam sandwich panels exhibit ductile behaviour when the glass microballoon contents are increased. This property is depicted in Figure 3 for all of the specimens. The SCSW-1 and SCSW-2 specimens exhibited a barrelling shape while the SCSW-3 to SCSW-5 specimens showed cracks at the edges of the skin. Furthermore, Shen et al. [9] determined that the sandwich panels for FRP/polyol-isocyanate foam had brittle behaviour during the compressive testing.

The compressive result for all of specimens indicates an initial linear elastic region followed by a mean plateau plastic region and a densification stage at the end of loading. Table 1 presents the modulus of elasticity ( $E_c$ ), maximum yield stress ( $\sigma_c$ ), maximum yield strain ( $\epsilon_c$ ) and their coefficient of variation (CoV's).

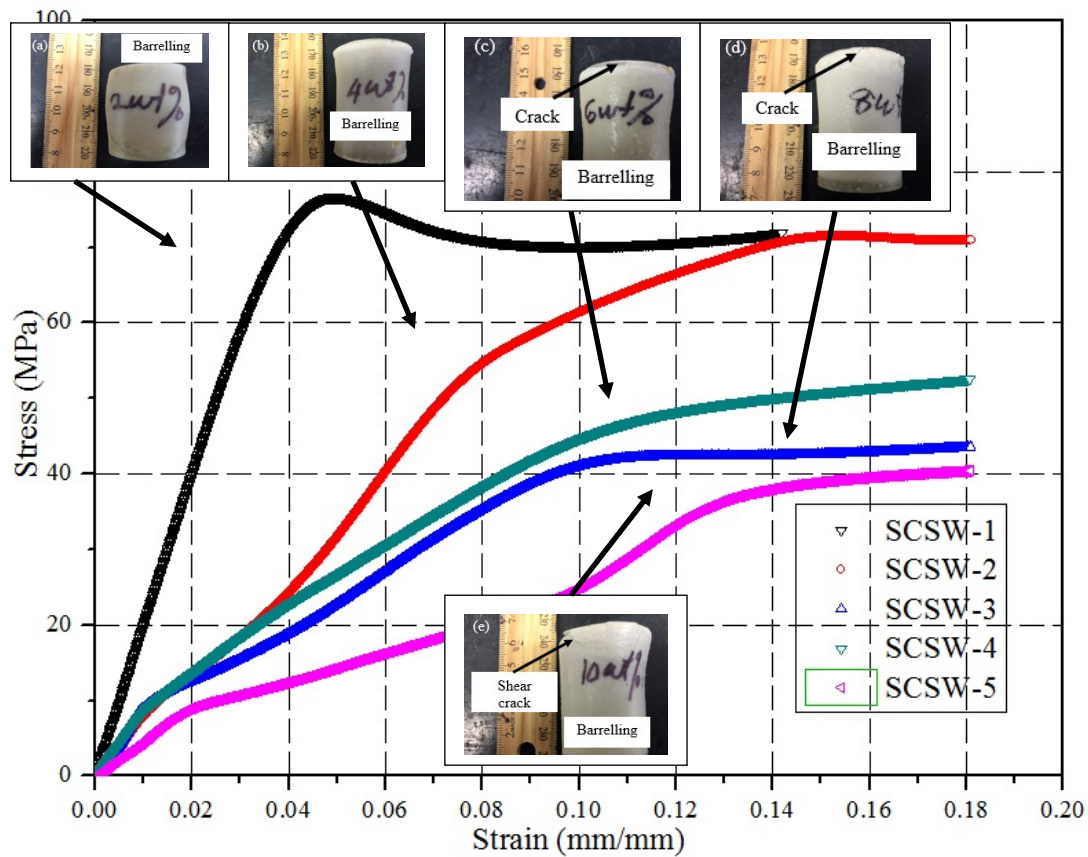


**Figure 3.** Representative overview of the stress-strain curve for compressive strength.

**Table 1.** Compressive characteristics for the syntactic foam sandwich panels.

Specimens	Glass Microballoon Content (wt%)	Modulus of Elasticity ( $E_c$ ) (MPa)	Max. Yield Stress ( $\sigma_c$ ) (MPa)	Max. Yield Strain ( $\epsilon_c$ ) (mm/mm)	CoV ( $E_c$ )	CoV ( $\sigma_c$ )	CoV ( $\epsilon_c$ )
SCSW-1	2	1614.18	77.04	0.14	0.04	0.01	0.02
SCSW-2	4	831.15	72.20	0.18	0.02	0.03	0.01
SCSW-3	6	402.85	52.55	0.18	0.05	0.03	0.02
SCSW-4	8	361.22	43.56	0.18	0.01	0.05	0.02
SCSW-5	10	194.92	40.41	0.18	0.08	0.01	0.01

\* CoV = Standard of deviation divided Mean ( $\sigma/\mu$ )

Generally, the compressive modulus of elasticity reduces with an increase in the glass microballoon contents in syntactic foam cores, which is demonstrated by SCSW-1. However, the compressive maximum yield stress and the maximum yield strain decrease when the glass microballoon contents increase in the syntactic foams. The ductility of the specimens can be clearly observed in SCSW-4 and SCSW-5, particularly the fractured area at the top edge with side cracks

when the glass microballoon content is increased, as indicated in Figure 4. Hence, all specimens indicate that their compressive properties decrease when the microballoon contents increase.

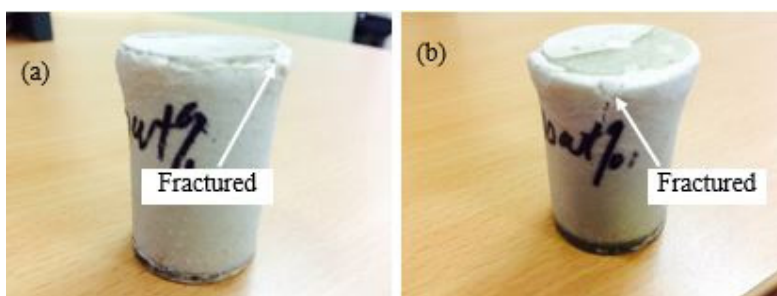


**Figure 4.** Fractured specimen at top edge after compressive testing for (a) SCSW-4; and (b) SCSW-5.

The compressive fractured mechanism can be divided into two types, which are known as barrelling and spalling. The specimens with low glass microballoon contents of 2 wt% to 6 wt% demonstrate barrelling mode. However, increasing the glass microballoon contents caused the syntactic foam behaviour to change to spalling mode, thus making it easy to fracture, especially near the top skin area. Furthermore, this crack started from the internal foam when the air void increased due to the higher glass microballoons contents. Nambiar and Ramamurthy [39] determined that the size and number of air voids could be varied with the foam volume unless the machine could determine the desired void contents in the specimens.

### 3.2. Tensile Properties

Generally, the tensile strength of the syntactic foam sandwich panels depicted in Figure 5 decreased when the glass microballoon contents increased. The detailed conditions of the failure modes state that the only acceptable failure modes for this test method are those internal to the sandwich construction (i.e., the core failure and the core-to-FRP skin bond failure) [40]. Based on ASTM C297/297M, four types of standard failure mode properties can be evaluated from the tensile testing: (a) core failure, (b) adhesive failure, (c) cohesive failure, and (d) facing tensile failure. Based on this finding, it is revealed that from testing the specimens, only failure modes (a), (b) and (c) were detected.

Compared to the peak stress values of the stress-strain curves, it can be observed that specimen STSW-2 exhibited the highest ultimate strength of 4.5 MPa. However, it cannot be considered as tensile failure because of occurring the failure mode (c) which is cohesive failure. Based on the photographs, it is revealed that the failure mode condition due to the bonding failure between the skin and the core clearly occurred for specimen STSW-2, as indicated in Figure 5. Therefore, it is not considered acceptable for determining the tensile strength in this case. Based on the observation of the STSW-1 and STSW-3 specimens in Figure 5, they exhibit syntactic foam core failure. The photographs illustrate that several air bubbles or voids occurred internally in the syntactic foam due to inadequate mixing during the preparation of the specimens. This failure mode is considered as

evidence of the tensile failure and supports the previous section on the compressive results for SFSW-1. Similar to the compressive result, the modulus of elasticity ( $E_t$ ), maximum yield stress ( $\sigma_t$ ), strain ( $\epsilon_t$ ) and coefficient of variations (CoV) are presented in Table 2.

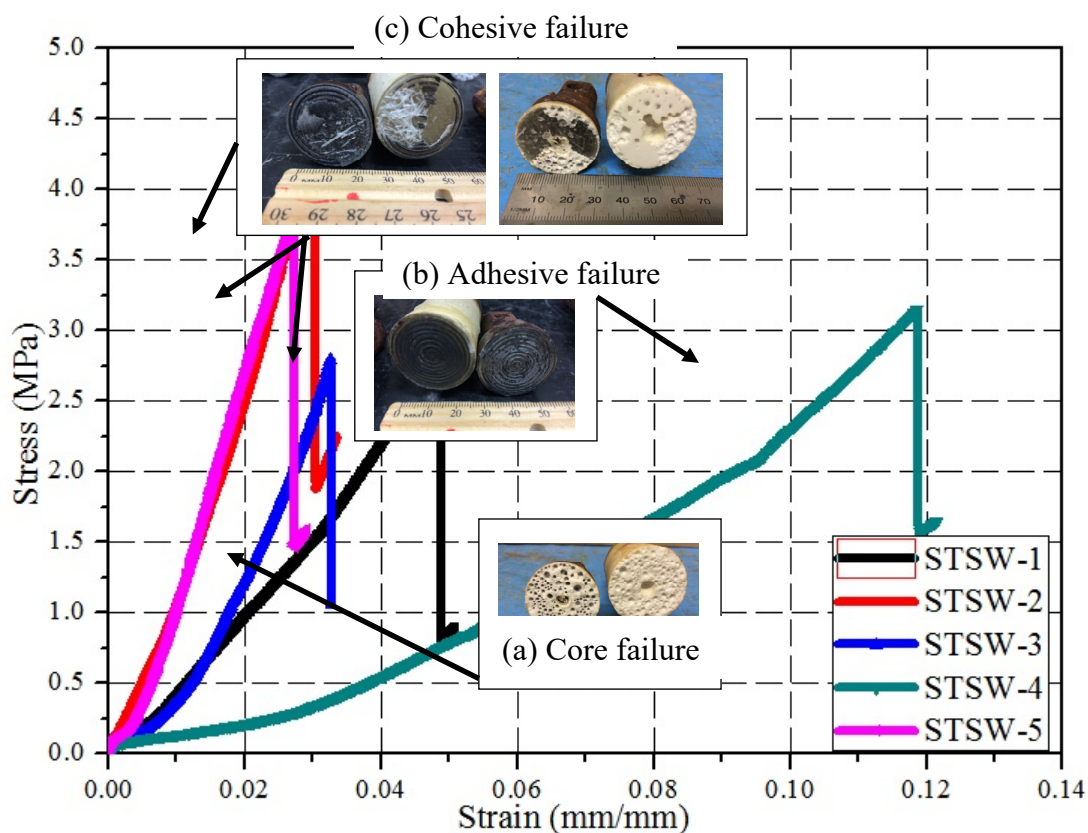


**Figure 5.** Representative overview of the stress-strain curve for tensile strength.

**Table 2.** Tensile characteristics for the syntactic foam sandwich panels.

Specimens	Glass microballoon content (wt%)	Modulus of Elasticity ( $E_t$ ) (MPa)	Ultimate Strength ( $\sigma_t$ ) (MPa)	CoV ( $E_t$ )	CoV ( $\sigma_t$ )
STSW-1	2	124.06	3.06	0.04	0.04
STSW-2	4	195.34	4.46	0.02	0.03
STSW-3	6	132.69	3.14	0.01	0.03
STSW-4	8	129.53	3.15	0.01	0.12
STSW-5	10	153.38	3.83	0.03	0.02

\* CoV = Standard of deviation divided Mean ( $\sigma/\mu$ )

From Table 2, it can be observed that no trend exists in the tensile modulus of elasticity, and the slope is highest for STSW-2 at 195.34 MPa. It can be observed that for specimens with a core failure mode, the modulus of elasticity should range from 120–135 MPa. It can be observed that specimen STSW-2 failed due to bonding failure, which is the area between the skin and the core, and it is also

known as cohesive failure. Furthermore, STSW-4 had the lowest modulus of elasticity of 129.53 MPa, which was due to adhesive failure. Because of this failure and having a maximum strain of 0.12 mm/mm, a longer elongation was noticed compared to other. A comparison of the difference in the modulus of elasticity between the compressive and tensile strengths may identify two possible reasons.

Gupta et al. [36] determined that one of the reasons was due to particle-matrix interfacial de-bonding. The existence of any de-bond causes a difference in the extent of stress transfer between the particle and the matrix. It has been shown in recent studies that the tensile modulus of elasticity is sensitive to the presence of de-bonding [8]. In comparison, under compressive loading conditions, de-bonding does not play an important role because the matrix is compressed on the particle, and separation occurs only in a small region in the direction transverse to the applied load. However, the presence of de-bonding could result in a slight decrease in the tensile modulus of elasticity, which occurred in this study. The second reason that plays an important role is the possibility of particle fracture under compressive loading conditions. It can be observed in Figure 5 that the compressive modulus of elasticity measurements can be obtained in the region where the load is approximately 40–60 MPa. Below this load level, it is difficult to determine the linearity of the stress-strain graphs. One of the reasons for this trend is that the sides of the compression specimens cannot be made perfectly parallel to each other, thus resulting in non-linearity at the onset of testing. This effect is minimised through careful sample preparation; however, it is difficult to completely eliminate it. Therefore, it can be concluded that based on the compressive and tensile testing for the modulus of elasticity, the foam is considered to be a bi-modulus material, where the tension modulus is different from the compression modulus of elasticity in the same direction. Shen et al. determined that  $E_t > E_c$  in FRP/polyol-isocyanate foam sandwich panels used in civil construction [9]. Furthermore, Cai [41] explained in his research that bi-modulus materials are widely used in concrete for civil engineering and cast iron for mechanical engineering.

### 3.3. Flexural Properties

#### 3.3.1. Flexure Properties of the GFRP Skin

Both the GFRP skin and sandwich panel properties were tested in this study. The GFRP skin coupons with a rectangular shape of length,  $L$  (~195 mm), width,  $W$  (~14 mm) and thickness,  $t$  (~2 mm). This GFRP skin property is useful for calculating the deflection of the sandwich panels.

A summary of the results for flexural 3-point bending of the GFRP skin is listed in Table 3. It can be observed that all 6 coupons exhibited stress-strain with an ultimate individual stress between 6–8 MPa. The gradient of the linear graph of the stress-strain provides the modulus of elasticity for the skin. From Figure 6, GFRP-6 has the highest  $E_s$  of 3.43 MPa. The low significant effects of the skin thickness may impact the possibility of achieving a higher modulus of elasticity. Generally, it is approximately 30% higher when compared to the  $E_s$  values for all of the coupons, as indicated in Table 3.

The influence of the skin thickness in this study should only slightly affect the higher modulus of elasticity for the 3-point bending (TBP) test for all coupons. Table 3 indicates that the difference

in the thicknesses between GFRP-2 and GFRP-6 is only 0.03 mm; however, the value of  $E_s$  is 25% higher than the rest, which is similar to the ultimate strength between the thick and thin thicknesses of the skin. Although GFRP-2 has a higher strength than GFRP-6, the thickness is not considerably different when compared to the rest. Therefore, the variation in the thickness of the skin has a lower impact on the ultimate strength and the modulus of elasticity of the skins. Shen et al. [9] determined that the bending strength is larger than the tensile strength for skin sandwich panels made from glass board REI FRP due to the thickness and uneven surface of the skins.

Using Table 3, the coefficient of variants (CoV's) can be calculated by dividing each individual value by the mean. The CoV's of the ultimate stress, CoV's of the modulus of elasticity and load maximum can be defined as 0.09, 0.13 and 0.12, respectively. Overall, GFRP-1 had the highest ultimate stress of 7.71 MPa, GFRP-2 had the maximum load of 0.220 kN, and GFRP-6 had the highest modulus of elasticity at 3.43 MPa. Furthermore, the behaviour of the GFRP skin can be described by investigating their extension during the flexural testing. Figure 6(b) illustrates that their properties vary with the thickness from 1.95 mm to 2.05 mm for GFRP-1 to GFRP-6.

**Table 3.** Flexural characteristics of the GFRP skin.

Specimens	Length L (mm)	Thickness t (mm)	Width W (mm)	Ultimate Stress $\sigma_{ult}$ (MPa)	Max. Load P (kN)	Modulus of Elasticity $E_s$ (MPa)	Stiffness M (N/mm)	Tangent modulus (MPa)
GFRP-1	192.00	2.00	13.49	7.71	0.208	2.78	49.72	48590
GFRP-2	193.00	1.98	14.70	7.56	0.220	2.58	47.53	43936
GFRP-3	196.00	2.03	15.37	6.12	0.190	2.40	52.39	42975
GFRP-4	194.00	2.05	13.43	6.46	0.177	2.72	54.76	49914
GFRP-5	195.00	1.97	14.65	6.94	0.200	2.60	50.09	47171
GFRP-6	195.00	1.95	11.20	7.13	0.155	3.43	65.52	49078

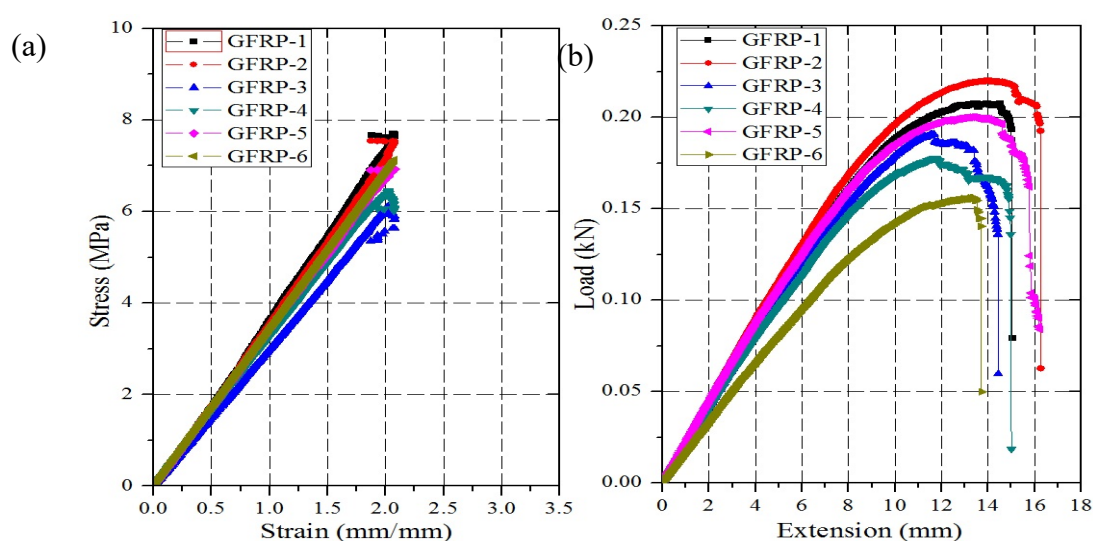


**Figure 6.** Representative plot graph of the GFRP skin for (a) Flexural testing; and (b) Load (kN)-Extension (mm).

The maximum load was achieved for GFRP-2 of 0.220 kN with an extension of 14.0 mm before it reached failure at 16.27 mm. Furthermore, the lowest load of 0.15 kN is achieved by GFRP-6 with an extension of 13.44 mm before it reaches failure at 13.72 kN. Specimens GFRP-1, GFRP-3 and GFRP-5 indicate that the loads varied from 0.18 kN to 0.21 kN. Generally, in this study, the thicknesses of the GFRP skin are not comparable with the load and extension along the flexural testing. From the stress-strain relation of flexural testing, the tangent modulus and the stiffness of the skin can be obtained [42]. The tangent modulus or modulus of elasticity in bending can be calculated using Equation (1) [43] as follows:

$$E_B = \frac{L^3 m}{4wt^3} \quad (1)$$

where L is the span length; m is the stiffness; w is the width of the skin; and t is the thickness of the skin. The stiffness of the skin can be obtained from the slope of the load-extension curve. Generally, the stiffness of the GFRP skins varied when thickness and width of the skin had different sizes for a fixed span length. It was revealed that a shorter width of GFRP contributed to increment of the modulus of elasticity and the stiffness properties especially specimen GFRP-6. The influence of the fibre glass sheet in the vinyl ester resin resulted in a different higher level of the strength of the skin, which also contributed as one of the factors. Furthermore, the randomness of the fibre orientation indicated an increase in the modulus of elasticity in the phenolic microsphere used as the filler in the epoxy resin, as demonstrated by Wouterson et al. [13].

### 3.3.2. Flexural Properties for Syntactic Foam Sandwich Panels

According to ASTM C393/393M, the failure mode can be classified as (a) unsymmetrical shear failure in the foam, (b) symmetrical shear failure in the foam, (c) de-bonding at the core-to-GFRP skin interface, (d) local collapse at the top GFRP surface, (e) local buckling of the top GFRP, which was attributed to the in-plane forces caused by the rounded surface of the loading cylinder making contact with the GFRP sheet and (f) local de-bonding between the top GFRP skin and the foam. The flexure for the syntactic foam sandwich panels are depicted in Figure 7. In this study, the core shear was revealed through different failure in the three point bending of flatwise sandwich panels (TFSW) and edgewise sandwich panels (TESW). Tensile cracks of the core were observed at the bottom of specimen (Figure 7). On the top of specimen TFSW-1, compressive failure also revealed due to de-bonding and unsymmetrical shear failure between skin and core as shown in Figure 7(a). Tensile cracks in the core failure were also observed at the bottom and side of specimen TESW-1 as shown in Figure 7(b). However, the occurrence of un-symmetrical skin in the edgewise position prevented the premature failure and made the syntactic foam sandwich panels failed in a ductile failure mode. Flexural core failure due to brittle syntactic foam with composition 10 wt% is clearly observed in Figure 7(c) for specimen TFSW-5. These cracks originated at the bottom of tensile skin and progressed with load application. The GFRP composite skins however bridged the cracked core together to prevent the intermediate failure during compressive mode. Figure 8 presents the typical stress-strain curves of the test specimens with shear failure. Generally, the slope of the graph slightly decreased when glass microballoons were added. From the graph, it was observed that the specimens

TFSW-1 and TESW-1 had similar higher shear stress with higher loading between 200–220 MPa and 3174–3175 N, respectively. The majority of test specimens exhibited shear failure of the foam during flexural testing. A small subset of the specimens failed from de-bonding and local collapse of the GFRP skin; therefore, the shear failure was assumed to be the dominant failure mechanism for three-point bending tests.

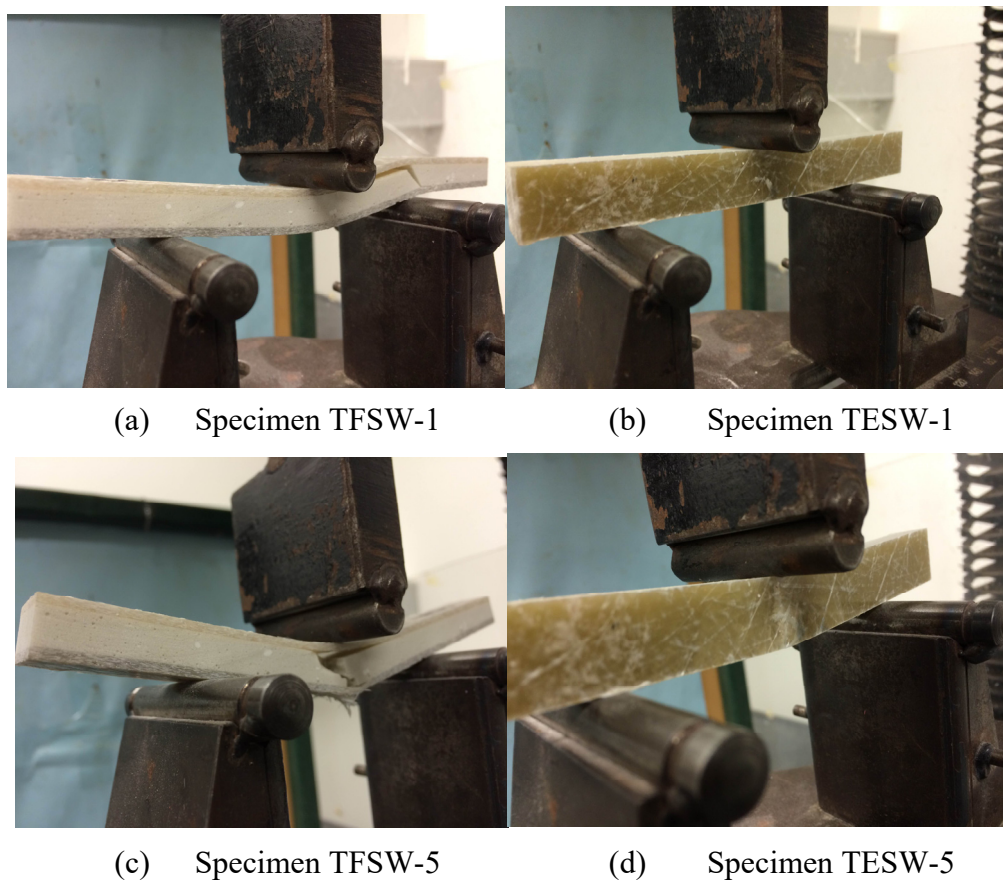


**Figure 7.** Representative failure of syntactic foam sandwich panels.

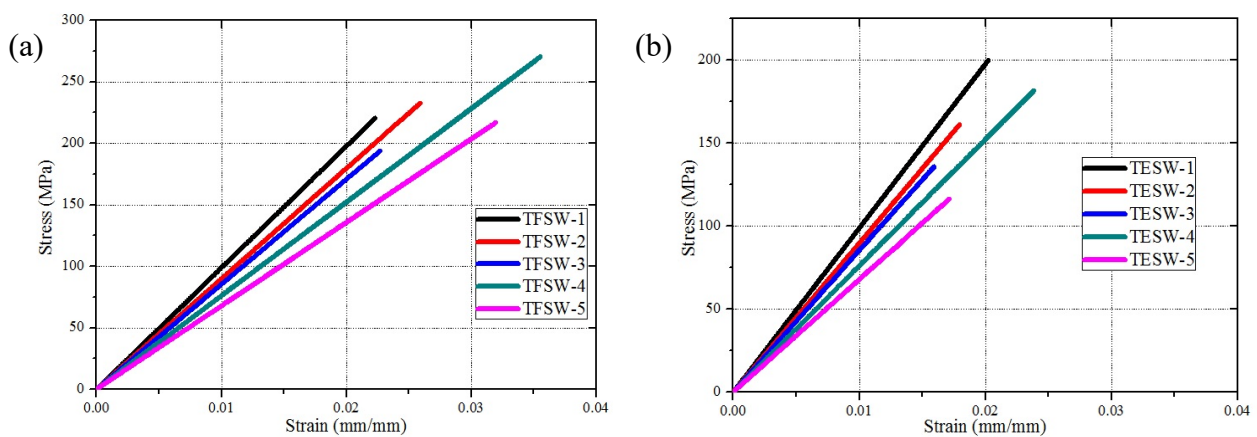


**Figure 8.** Representative result of the stress-strain curve for flexural strength; (a) Flatwise, (b) Edgewise.

The formula for the core shear ultimate strength can be determined by Equation (2), which is obtained from ASTM C393/C393M [44]. Furthermore, the formula for the facing stress can be derived using Equation (3). Hence, the calculated values explained the behaviour of the syntactic foam sandwich panel, as indicated in Table 4.

$$\tau_{ult} = \frac{F_{max.}}{(D+c)B} \quad (2)$$

$$\sigma_{fc} = \frac{F_{max.}S}{2t(D+c)B} \quad (3)$$

where  $F_{max.}$  is the maximum force prior to failure (N);  $D$  is the thickness of the syntactic foam sandwich panels (mm);  $c$  is the core thickness (mm);  $t$  is the nominal facing thickness (mm);  $B$  is the width of the syntactic foam sandwich panels; and  $S$  is the span length (mm).

From Table 4, the ultimate stress,  $\tau_{ult}$  and the facing stress,  $\sigma_{fc}$  show increment with the highest thickness of sandwich panels particularly flatwise shear stress mode for TFSW-1. In comparison, a different result was found for edgewise mode position for TESW-5 though it was thicker than this specimen with  $\tau_{ult} = 6.89$  MPa and  $\sigma_{fc} = 258.46$  MPa, respectively. This phenomenon occurred the failure mode as delamination between GFRP skin and syntactic foam core. The foam core with a very thin layer remained adhered to the skin in the case of matrix de-bonding.

**Table 4.** 3-point bending (TBP) flexural characteristics for the flatwise (TFSW) and edgewise (TESW) syntactic foam sandwich panels.

Specimens	t (mm)	L (mm)	B (mm)	l (mm)	$\sigma_{max.}$ (MPa)	$F_{max}$ (N)	$\tau_{ult}$ (MPa)	$\sigma_{fc}$ (MPa)
TFSW-1	13.00	75	11.25	120	220	3174	11.29	423.29
TFSW-2	10.86	75	13.95	120	233	2807	9.71	364.11
TFSW-3	12.17	75	13.98	120	194	3570	10.08	377.92
TFSW-4	9.65	75	14.70	120	271	2785	9.88	370.33
TFSW-5	11.27	75	15.45	120	217	2989	9.20	344.95
TESW-1	13.30	75	11.80	120	200	3175	10.51	394.10
TESW-2	12.07	75	10.96	120	161	1924	7.59	284.55
TESW-3	14.60	75	12.40	120	136	2770	7.92	297.04
TESW-4	10.30	75	15.30	120	181	2135	7.12	266.93
TESW-5	14.80	75	11.14	120	116	2196	6.89	258.46

Note:  $t$ : Foam thickness,  $L$ : span length,  $B$ : Nominal width,  $l$ : Nominal length,  $\sigma_{max.}$ : Max. Stress,  $F_{max.}$ : Max. Load,  $\tau_{ult}$ : Ultimate core shear strength,  $\sigma_{fc}$ : Facing Stress,  $E_m$ : Modulus of Elasticity

### 3.3.3. Flexural Stiffness Properties for Syntactic Foam Sandwich Panels

An evaluation of the flexural stiffness of the syntactic foam sandwich panels is determined using the flexural stiffness for flatwise equation, particularly for beams. Manalo et al. [45] used the

flatwise beam equation, which considers both the skin and core properties for the flexural behaviour of glue-laminated fibre composite sandwich beams. The flatwise beam sandwich panel equation for flexural stiffness (EI) can be depicted in Equation (3) while the flexural stiffness for edgewise beam is shown in Equation (4) as follows:

$$EI_{\text{flatwise}} = \sum_{i=1}^n \left[ \left( \frac{Bt_s^3}{12} + Bt_s d_s^2 \right) E_s + \left( \frac{Bt_c^3}{12} + Bt_c d_c^2 \right) E_c \right] \quad (3)$$

$$EI_{\text{edgewise}} = \frac{nD^3}{6} \left( t_s E_s + \frac{t_c}{2} E_c \right) \quad (4)$$

where B is the width of panel;  $t_s$  is the thickness of the skin;  $t_c$  is the thickness of the core;  $d_s$  and  $d_c$  are the distances from the centre of the skins and the core to the neutral axis of the glued section, respectively;  $E_s$  and  $E_c$  are the modulus of elasticity of the skin and core, respectively; and D is thickness sandwich panels while n is the number of glue-laminated composite sandwiches. In this study,  $n = 1$  is fixed because there is only 1 layer, and  $d_c = 0$  at the centre of the core syntactic foam. All of the calculations were performed by assuming that there was no occurrence of the interlayer slip, and the laminated sandwich acted as a solid perfect bonding or was directly mounted between the skin and the core to avoid the secondary effects on the syntactic foam sandwich panels. Manalo et al. [45] introduced the effective stiffness formula, EI effectiveness, which is derived from the deflection formula. Furthermore, Islam and Kim [25] introduced the effective stiffness of a syntactic foam beam using Equation (5) as follows:

$$EI_{\text{eff.}} = \frac{EI_{\text{flatwise}}}{B} \quad (5)$$

The TPB testing had a similar mechanism for simply supported beams to determine the deflection in this study. Hence, the deflection for a simple beam can be derived using Equation (6), which is commonly used for static mechanical engineering calculations.

$$v_{\text{Def.}} = \frac{FS^3}{48EI_{\text{flatwise}}}, v_{\text{Def.}} = \frac{FS^3}{48EI_{\text{edgewise}}} \quad (6)$$

where F is the force perpendicularly directed to the specimens; and S is the midspan. According to Islam and Kim [25], the flexural modulus for beam can be determined by using Equation (7) as below;

$$E_{\text{flex}} = \frac{S^3 M}{4BD^3} \quad (7)$$

where M is the slope of the Load-Deflection graph. The resulting parameters  $E_c$ ,  $E_{\text{flatwise}}$  and  $E_{\text{eff}}$  are listed in Table 5.

From Table 5, the modulus of elasticity ( $E_{\text{flex}}$ ) generally decreased when the glass microballoons content increased for the syntactic foam sandwich panels. This result was observed when the thickness of the syntactic foam sandwich panels was thinner compared to all of the specimens, e.g., FLSW-4 had a lower stiffness (EI) and a lower effective stiffness ( $E_{\text{eff}}$ ) for both

flatwise and edgewise position. The reduction was nearly 53% when compared for all stiffness values, and it had a significant effect on the syntactic foam sandwich panels as well. In addition, a lower difference in percentage was found between flatwise and edgewise specimens for both EI (0.5%) and  $EI_{\text{eff}}$  (0.7%), respectively. It was suggested that shear deformation could have contributed to the total deformation of the composite syntactic foam sandwich panels in the flatwise position due to the decreased thickness ratio. Modulus of elasticity also varied with different thickness of syntactic foam core. Generally, all the specimens showed decrement in the modulus of elasticity when glass microballoons were added in syntactic foam. From the result, the highest value of  $E_{\text{flex}}$  was led by lower glass microballoon content with 2 wt% for flatwise and edgewise specimen FLSW-1 and FESW-1. The similar result was also observed in previous section for modulus of elasticity in stress-strain curve for flexure properties. The decreasing of modulus in flatwise position clearly indicated that GFRP skin near the neutral axis of the section did not contribute as much stiffness as the outermost skin. No trend was found for edgewise modulus of elasticity but it can be seen that the thin core thickness had lower modulus of elasticity belonging to FESW-4 at 578.76 MPa. This clearly shows that the modulus of elasticity in the flatwise and edgewise position is not only affected by core thickness but also due to the glass microballoon content as isotropic materials behaviour adopted in the syntactic foam.

**Table 5.** Predicted and calculated EI,  $EI_{\text{eff}}$ , flexural stiffness for the syntactic foam sandwich panels.

Specimens	Modulus of Elasticity $E_{\text{flex}}$ (MPa)	Flexural Stiffness EI ( $\times 10^6 \text{ N}\cdot\text{mm}^2$ )	Difference in EI (%)	Effective Stiffness $EI_{\text{eff}}$ ( $\times 10^6 \text{ N}\cdot\text{mm}^2$ )	Difference in $EI_{\text{eff}}$ (%)
FLSW-1	972	16017600	17	1423786	28
FESW-1	1288	23840673		2020396	
FLSW-2	840	10012245	31	717723	30
FESW-2	1134	14572267		1329586	
FLSW-3	842	17942471	25	1283438	31
FESW-3	1171	30133449		2430116	
FLSW-4	648	6377686	0.5	415213	0.7
FESW-4	546	6450756		421618	
FLSW-5	637	8774060	50	567533	60
FESW-5	1051	25307707		2271787	

### 3.3.4. Load-Deflection Properties for Syntactic Foam Sandwich Panels

The load and midspan deflection behaviour of the individual syntactic foam sandwiches under 3-point static bending is depicted in Figure 9. It is demonstrated that the load of specimen FLSW-3 increased nearly 3 times higher than other specimens with the load up to final failure for both flatwise and edgewise position. The deflection shows lower at 14 mm and 8.5 mm for flatwise and edgewise position, respectively. This graph also illustrates that FLSW-3 demonstrated a higher load

and extended the stretch 35% when compared with other foams at 14 mm and 45% at 9 mm for flatwise and edgewise, respectively. There was an increase in the deflection proportional to an increase in the applied load, which may be due to the progressive failure of the non-horizontal skin thickness. Generally, the specimens failed at an applied load of between 2500 N to 3500 N for flatwise while 1900 N to 3100 N for edgewise position with a midspan deflection of 75 mm. The load of specimens for both flatwise and edgewise position FLSW-4 exhibiting lower load deflection failure also increased linearly with the deflection from 19 to 21 mm but showed a reduction in the stiffness at a load of approximately between 2200 N to 2600 N due to the flexural tensile cracking of the core.

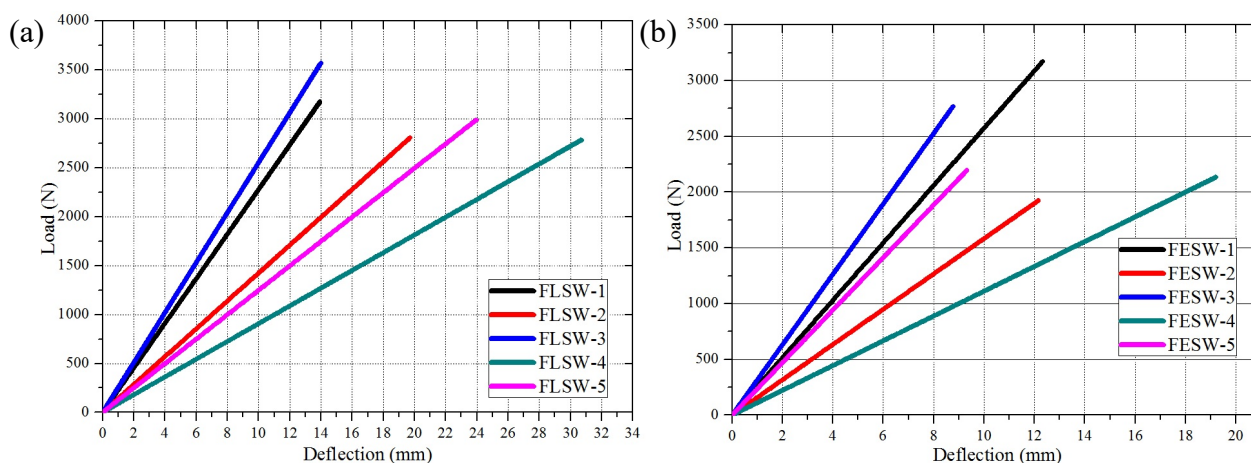


**Figure 9.** Representative graph for Load vs. Deflection; (a) Flatwise (b) Edgewise for syntactic foam sandwich panels.

Additionally, Manalo et al. [45] determined that tensile cracking occurred in the core when it was tested using edgewise testing of the sandwich panels. In this study, the deflection of the syntactic foam sandwich panels slightly increased when the stiffness and the sandwich thickness decreased. Furthermore, Islam and Kim [41] determined that the low density of syntactic foam indicates tremendous results in the higher deflection for different starch to water ratios. However, Manalo et al. [40] indicated that the load-deflection composite sandwich beams tested in the flatwise position failed due to the brittle and ductile properties of the sandwich panels. Similar to the syntactic foam sandwich panels, this study determined that the load-deflection increased when the glass microballoon content increased in a core material. Therefore, a significant effect on the properties of the core density as well as increased glass microballoon contents affected the sandwich panel properties during fabrication of the syntactic foam.

In this study, all of the specimens demonstrated failure in brittle fracture behaviour mode, which was revealed at the end of testing in the elastic region for both flatwise and edgewise position. A similar trend was also revealed by Maharsia et al. [42], who fabricated a hybrid syntactic foam using epoxy resin as the matrix resin. The thickness of the core resulted in this specimen having still the highest strength among all of the specimens. Although the skin thickness for all of the specimens was on average only 2.0 mm; however, because the thickness of this foam is less than 10 mm, it may

make it stronger than other foams. The maximum force generated at the top skin of the FLSW-4 specimen had a similar magnitude to that at the bottom skin through this extension. Based on a comparison among the different thicknesses, the following results can be observed. First, using a thicker foam core does not necessarily produce the highest pressure yield before fracture. Table 4 indicates that a thicker foam size between 10–12 mm produces a lower force and is easier to fracture. However, a core foam less than 10 mm results in a significantly stronger force. Secondly, this phenomenon may also be attributed to variations in the porosity and number of voids in the syntactic foam. The number of voids and porosity can vary with the foam density.

### 3.4. SEM for Syntactic Foam Sandwich Panel Structure Properties

#### 3.4.1. Effects on the GFRP Skin

Additionally, the SEM observation of the fibre glass sheet as a skin is performed in this study. Figure 10(a) illustrates an overview of a unidirectional fibre glass sheet embedded in vinyl ester resin as the matrix material. It is revealed that several sizes of fibre glass were cut and remained in the matrix resin. Furthermore, fractured and de-bonded fibres, matrix deformation, and de-bonded and crushed fibres were observed. Figure 10(b) confirms the random orientations of the glass fibre sheet because both perpendicularly and longitudinally orientated fibres are observed.

The SEM indicates that the direction of fibres tend to the higher FGS skin, which is stronger in only one direction. Gupta et al. [46] determined that a fibre orientation with two different directions recorded a better reflection incline in more than one direction. Relatively, this may be caused by the strength syntactic foam with and without fibres. Additionally, this technique can drastically optimise the void contents in syntactic foam to 4% and result in a higher strength. Thus, it can be clearly demonstrated that the role of the fibres will increase the fracture toughness via the creation of an extensive structure and de-bonding activity. This fibre orientation will lead to an increase in the stress field overlapping between the fibres, thus resulting in an enhanced plasticity of the fracture toughness.

#### 3.4.2. Effects on the Syntactic Foam Sandwich Panels

The compressive specimens are used to analyse the fracture microstructure mechanism in this study. Maharsia et al. [42] used different types of microballoons to explain the mechanism fracture for final compressive testing. Sandwich panels with a lower glass microballoon content (2 wt%) core, such as SCSW-1, resulted in a higher compressive strength, as indicated in Table 1. This result can also be observed by observation in the SEM photograph in Figure 10(c), where the vinyl ester resin reacts as a plastic region embedded with fewer debris glass microballoons and void contents. The interfacial bonding between the glass microballoon and the matrix resin remains strong. The absence of debris indicates that a lower crushing and de-bonding phenomenon occurred after compressive testing. In this specimen, it is difficult to determine the de-bonding between the filler glass microballoon and the matrix resin, and the connection between them remains strong.

The compressive observation continued for specimens with increased glass microballoon content, particularly 4–8 wt%, i.e., specimens SCSW-2 to SCSW-4. The compressive strength for these specimens decreased to nearly 50% of the value of those with lower glass microballoon contents, which was SCSW-1. The spreading of the debris and fractured glass microballoons is illustrated in Figure 10(d). The syntactic foam is more brittle and has numerous pores, which attempt to include their debris into the broken glass microballoon and voids area. Additionally, whiskers from the matrix resin can be observed, including their twist hackle line. It was also observed that the mean plateau region for the compressive curve in Section 3.1 indicates that the plasticity of the matrix resin remains, thus achieving a maximum stress longer than the other specimens.

Figure 10(e) depicts that the de-bonding between the filler glass microballoon and matrix resin occurred frequently. The number of crushed glass microballoons and debris kept increasing, as observed in SCSW-3. This phenomenon resulted in the highest number present in any fractured plan and increased the possibilities of crack bridging occurring in the syntactic foams. Azimi [47] discovered that the same characteristic occurred in hybrid syntactic foams. All of the fractured particles surrounded the glass microballoon and the cavity pore area. Severe de-bonding of the glass microballoons was observed in Figure 10(f), where nearly 80% de-bonding occurred for SCSW-5. Furthermore, this phenomenon resulted in a lower strength of compressive failure and difficulty in identifying their mean plateau, and the dissatisfactions modes of the syntactic foams became 48% lower than the highest strength value. The segregation of the entrapped air voids was observed severely in this specimen, which may have resulted in the reduction in strength as well.

#### 3.4.3. Effects on the Stiffness Syntactic Foam Sandwich Panels

The 3-point bending specimens are used to analyse the stiffness mechanism in this study, particularly specimen FLSW-4. An overview of the aggregates between the FGS skin and the cores for FLSW-4 is depicted in Figure 10(g). The Figure clearly indicates that the FGS skin can join and stick to the syntactic foam core with minimal tolerance because both the flexural and effective stiffness had lower values of  $6377686.12 \times 10^6 \text{ N}\cdot\text{mm}^2$  and  $415213.94 \times 10^6 \text{ N}\cdot\text{mm}^2$ , respectively. The advantages of this sandwich panel are related to the thickness of the cores, which results in the crack propagation between the skin and the core having less of an impact during flexural testing. Furthermore, Figure 10(g) indicates that the deflection of FLSW-4 withstood a higher force to failure at 3500 N with a deflection of 14 mm. This force was considered to be the highest among all of the specimens and achieved a bearing loading application. Shen et al. suggested that controlling the thickness of the foam and skin can improve the stiffness boundary condition [9]. Using the higher magnification micrograph, Figure 10(h) indicates that the aggregate size can be measured to be approximately 1–2  $\mu\text{m}$  in size. This phenomenon may occur due to the degradation in the matrix material during the deformation and fracture processes in flexural testing. This result implies that during the loading process, most of the stress in the composite is withstood by the matrix material, whose flexural cracking determines the composite failure.

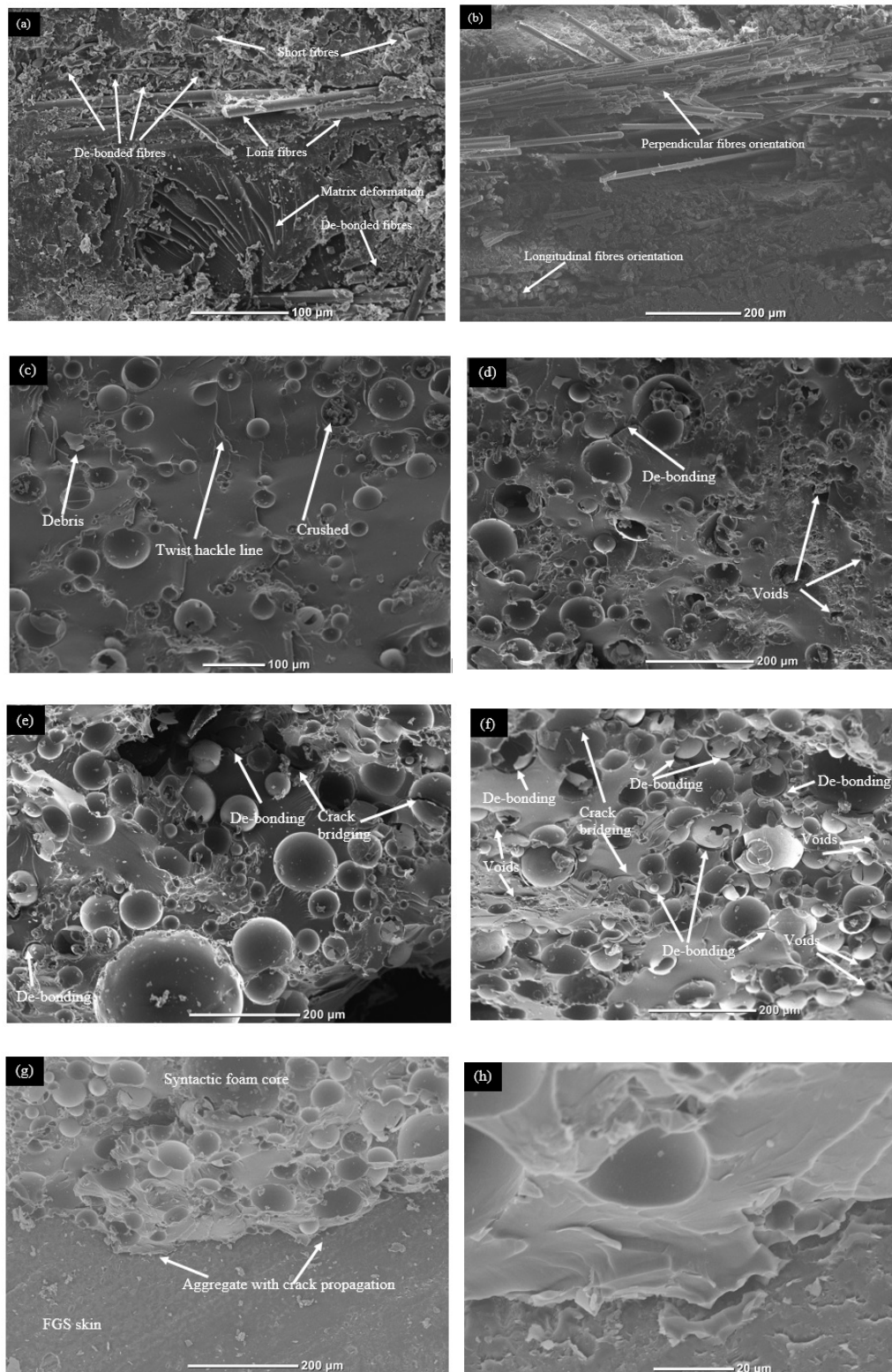


**Figure 10.** SEM images for (a) Fractured fibres in the matrix resin; and (b) Different fibre orientation embedded in the matrix resin. Fractured glass microballoons distributed in the vinyl ester resin for (c) SCSW-1; (d) SCSW-2; (e) SCSW-3; (f) SCSW-5; (g) Crack propagation during flexural testing for FLSW-4; and (h) Higher magnification view identified the aggregate size of 1–2  $\mu\text{m}$ .

#### 4. Conclusions

The fabrication and characterisation of syntactic foam core sandwich panels made from GFRP (glass fibre reinforced plastic) skin and glass microballoons with different weight percentages of glass microballoon contents (2–10 wt%) demonstrated the following:

- The mechanical behaviour of the syntactic foam sandwich panels in relation with the properties of constituent materials has been studied.
- The compressive strength of the sandwich panels is significantly affected by a low density foam core, as well as their modulus of elasticity and maximum stress value, particularly with 2.0 wt% of glass microballoon.
- The tensile failure of the sandwich panels is also significantly affected by lower glass microballoon contents (2 wt%). The core failure was clearly observed compared to other failure modes, such as cohesive and adhesive failure modes.
- The selection of the GFRP skin also contributed as a primary factor to the fabrication of sandwich panels as well as considering the total density of the sandwich panels.
- The flexural testing of the syntactic foam sandwich panels indicated a higher strength when the glass microballoon contents are increased in the core materials compared to that in un-symmetrical shear failure mode.
- Porosity content, de-bonding of glass microballoon and crack bridging might contribute to the different values of the flexural stiffness of sandwich panels. The different thickness of syntactic foam core also has important role in the deflection between GFRP skin and syntactic foam core with varied contents of glass microballoon.

The results of the load-deflection behaviour of syntactic foam core sandwich panels indicated a significant effect on the core properties with higher deflection when the glass microballoon content is increased, such as to 8 wt% and 10 wt%.

#### Acknowledgements

The authors would like to thank Majlis Amanah Rakyat (MARA), Malaysia and Universiti Kuala Lumpur Malaysian Institute of Marine Engineering Technology, Malaysia for providing a scholarship to the first author of this study.

#### Conflict of Interest

The authors declare that there is no conflict of interest regarding the publication of this manuscript.

#### References

1. Klemmner D, Sendjarevic V (2004) Handbook of polymeric foams and foam technology, Munich, Germany: Carl Hanser Verlag.

2. Khemani KC (1997) Polymer Foams: An Overview. Polymeric Foams. ACS Symposium Series, Washington, DC: American Chemical Society.
3. Zenkert D (1995) An introduction to sandwich constructions. *Engineering materials advisory services*, London.
4. Allen H (1969) Analysis and design of structural sandwich plates: Franklin Book Co.
5. Gay D, Hoa S (2007) Composite materials: design and applications. 2nd Eds, Taylor & Francis group, LLC.
6. Quilter A (2006) Composites in aerospace applications. ESDU International. Canada: An IHS White Paper.
7. Johnson CF, Rudd C (1998) Manufacturing process selection for composite components, Cambridge Press.
8. Tagliavia G, Porfiri M, Gupta N (2009) Vinyl ester-glass hollow particle composites: dynamic mechanical properties at high inclusion volume fraction. *J Compos Mater* 43: 561–582.
9. Shen SY, Masters FJ, Upjohn HL, et al. (2013) Mechanical resistance properties of FRP/polyol-isocyanate foam sandwich panels. *Compos Struct* 99: 419–432.
10. Mostafa A, Shankar K, Morozov EV (2013) Insight into the shear behaviour of composite sandwich panels with foam core. *Mater Design* 50: 92–101.
11. Salleh Z, Islam M, Ku H (2014) Study on Compressive Properties of Syntactic Foams for Marine Applications. *J Multifunctional Compos* 2: 21–27.
12. Gupta N, Priya S, Islam R, et al. (2006) Characterization of mechanical and electrical properties of epoxy-glass microballoon syntactic composites. *Ferroelectrics* 345: 1–12.
13. Wouterson EM, Boey FYC, Hu X, et al. (2007) Effect of fiber reinforcement on the tensile, fracture and thermal properties of syntactic foam. *Polymer* 48: 3183–3191.
14. Shankar R, Sankaran S (2005) Short beam three point bend tests in syntactic foams. Part I: Microscopic characterization of the failure zones. *J Appl Polym Sci* 98: 673–679.
15. Karthikeyan C, Sankaran S, Kumar M, et al. (2001) Processing and compressive strengths of syntactic foams with and without fibrous reinforcements. *J Appl Polym Sci* 81: 405–411.
16. Wouterson E, Boey F, Hu X, et al. (2004) Fracture and impact toughness of syntactic foam. *J Cell Plast* 40: 145–154.
17. Bardella L, Genna F (2001) Elastic design of syntactic foamed sandwiches obtained by filling of three-dimensional sandwich-fabric panels. *Int J Solids Struct* 38: 307–333.
18. Bardella L, Genna F (2001) On the elastic behavior of syntactic foams. *Int J Solids Struct* 38: 7235–7260.
19. Sagi-Mana D, Narkis M, Siegmann A, et al. (1998) The effect of marine environment on a vinyl ester resin and its highly filled particulate quartz composites. *J Appl Polym Sci* 69: 2229–2234.
20. Rajapakse Y, Hui D (2008) Marine composites and sandwich structures. *Compos Part B-Eng* 39: 1–4.
21. Rajapakse Y, Hui D (2004) Marine composites: foreword. *Compos Part B-Eng* 35: 447–450.
22. Fam A, Sharaf T (2010) Flexural performance of sandwich panels comprising polyurethane core and GFRP skins and ribs of various configurations. *Compos Struct* 92: 2927–2935.
23. Cheng Q, Lee H, Lu C (2006) A numerical analysis approach for evaluating elastic constants of sandwich structures with various cores. *Compos Struct* 74: 226–236.

24. Sharaf T, Shawkat W, Fam A (2010) Structural performance of sandwich wall panels with different foam core densities in one-way bending. *J Compos Mater* 44: 2249–2263.
25. Islam MM, Kim HS (2007) Novel syntactic foams made of ceramic hollow micro-spheres and starch: theory, structure and properties. *J Mater Sci* 42: 6123–6132.
26. Awad ZK, Aravinthan T, Manalo A (2012) Geometry effect on the behaviour of single and glue-laminated glass fibre reinforced polymer composite sandwich beams loaded in four-point bending. *Mater Design* 39: 93–103.
27. Zhang J, Kikuchi N, Li V, et al. (1996) Constitutive model of polymeric foam material subjected to dynamic crash loading. *Int J Impact Eng* 21: 369–386.
28. Maji A, Schreyer H, Donald S, et al. (1995) Mechanical properties of polyurethane-foam impact limiters. *J Eng Mech* 121: 528–540.
29. Ranade A, Hiltner A, Baer E, et al. (2004) Structure–property relationship in coextruded foam/film microlayers. *J Cell Plast* 40: 497–507.
30. Wouterson E, Boey F, Hu X, et al. (2005) Specific properties and fracture toughness of syntactic foam: effect of foam microstructures. *Compos Sci Technol* 65: 1840–1850.
31. Ruan D, Lu G, Chen F, et al. (2002) Compressive behavior of aluminum foams at low and medium strain rates. *Compos Struct* 57: 331–336.
32. Sheng H, Gang Z (1999) The mechanical behavior of foamed aluminium. *J Mater Sci* 34: 291–299.
33. Avalle M, Belingardi G, Ibba A (2007) Mechanical models of cellular solids: parameters identification from experimental tests. *Int J Impact Eng* 34: 3–27.
34. Ashby M (1983) The mechanical properties of cellular solids. *Metall Mater Trans A* 14: 1755–1769.
35. Peroni L, Avalle M, Peroni M (2008) The mechanical behavior of aluminum foam structures in different loading conditions. *Int J Impact Eng* 35: 644–658.
36. Gupta N, Ye R, Porfiri M (2010) Comparison of tensile and compressive characteristics of vinyl ester/glass microballoon syntactic foams. *Compos Part B-Eng* 41: 236–245.
37. Viot P, Beani F, Lataillade J (2005) Polymeric foam behavior under dynamic compressive loading. *J Mater Sci* 40: 5829–5837.
38. Lin H (1997) The structure and property relationships of commercial foamed plastics. *Polym Test* 16: 429–443.
39. Nambiar E, Ramamurthy K (2007) Air-void characterization of foam concrete. *Cement Concrete Res* 37: 221–330.
40. ASTM C297/C297M-04 (2004) Standard test method for flatwise tensile strength of sandwich constructions, USA.
41. Cai K (2010) Effects of the Properties of Bi-modulus Material on Stiffness Design. Intelligent Computation Technology and Automation (ICICTA), 2010 International Conference on. IEEE 2: 192–195.
42. Maharsia R, Gupta N, Jerro HD (2006) Investigation of flexural strength properties of rubber and nanoclay reinforced hybrid syntactic foams. *Mat Sci Eng A* 417: 249–258.
43. ASTM D790-03 PA (2003) Standard Test Methods for Flexural Properties of Unreinforced and Reinforced Plastics and Electrical Insulating Materials, USA: ASTM International.

44. ASTM C393/C393M (2012) Standard Test Method for Core Shear Properties of Sandwich Constructions by Beam Flexure., West Conshohocken, PA 19428–2959, USA: ASTM International.
45. Manalo AC, Aravinthan T, Karunasena W (2010) Flexural behaviour of glue-laminated fibre composite sandwich beams. *Compos Struct* 92: 2703–2711.
46. Gupta N, Karthikeyan CS, Kishore SSa (1999) Correlation of processing methodology to the physical and mechanical properties of syntactic foams with and without fibers. *Mater Charact* 43: 271–277.
47. Azimi H, Pearson R, Hertzberg R (1996) Polymer Engineering Science.



**AIMS Press**

© 2016 Md Mainul Islam, et al., licensee AIMS Press. This is an open access article distributed under the terms of the Creative Commons Attribution License (<http://creativecommons.org/licenses/by/4.0>)